Research on Self-Adaptive Algorithm of Transient Performance Analysis for DC Electronic Instrument Transformer Calibration

Dong Li, Ruoyu Wu, Han Liu, Junchang Huang, Haoliang Hu, Qi Nie, and Dezhi Chen

***Abstract*— The dc electronic instrument transformers (DCEITs) are widely used in the voltage-source converter-based high-voltage direct current (VSC-HVdc) transmission system to measure the bus voltage or current and should be of accurate and quick transient response. The transient performance of the DCEIT needs to be calibrated using a calibrator. The existing schemes are difficult to recognize different transient step responses automatically and usually require human intervention, which limits their flexibility and applicability. Besides, the accuracy of the calculated results is affected by human factors. A self-adaptive algorithm of transient performance analysis is proposed. It recognizes the characteristics of the transient step response based on wavelet analysis and distinguishes the steady-state and step intervals automatically. Then, it evaluates and finds the stable data segments in the steady-state intervals adaptively to calculate the high and low steady-state values. Finally, the data in the step interval are interpolated to search the feature points of the waveform, and then, the transient response parameters are calculated according to the coordinates of the feature points. In the validation stage, six kinds of step response waveforms are generated by MATLAB to test the performance of the proposed algorithm. Compared with the boundary window method, the proposed algorithm could recognize the characteristics of the tested waveforms automatically and achieve more accurate analyses of transient performance. In addition, a calibrator prototype based on the proposed algorithm is developed, and some tests are carried out at the National Center for High Voltage Measurement (NCHVM) in China, whose results verify the feasibility of the algorithm.**

***Index Terms*— DC electronic instrument transformer (DCEIT), step response, transformer calibrator, transient performance, wavelet analysis.**

I. Introduction

THE voltage-source converter-based high-voltage direct current (VSC-HVdc) technology has been piloted in the integration of renewable clean energy resources and island power supply in China [1]. Large transient current may be generated due to dc side fault in the VSC-HVdc system, which requires the dc voltage and current detection instruments [usually called dc electronic instrument transformers (DCEITs)] of accurate and quick dynamic response characteristics, so as to meet the need of quick protection and ensure the reliable operation of the VSC-HVdc system [2]–[4]. The National Standard GB/T 26216.1-2019 puts forward specific requirements of the DCEIT transient performance, mainly involving the rise time, overshoot, and setting time [5].

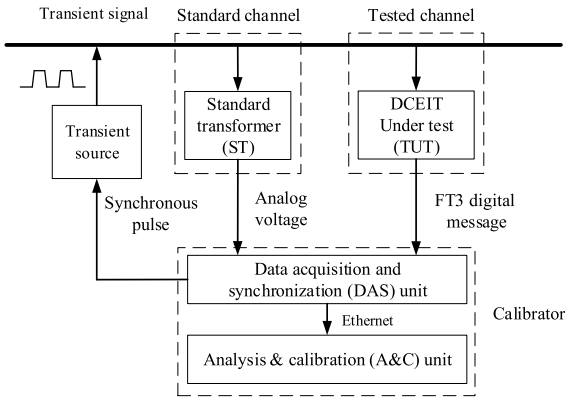

Fig. 1. Transient performance calibration scheme for DCEIT.

Before putting it into operation, the transient response performance of the DCEIT needs to be calibrated [6]–[13]. The direct comparison principle is generally adopted in the calibration, as shown in Fig. 1. First, the transient source usually delivers an approximate square-wave signal in practice to the standard transformer (ST) and the DCEIT under test (TUT) simultaneously, whose output signals will be accepted by the calibrator synchronously. These output signals could be called square-wave responses, and each cycle of the waveform can be regarded as a step response. Next, the analysis & calibration (A&C) unit calculates the high and low steady-state values to obtain the amplitude of the transient response waveform, and then, the feature points of specific amplitude percentages (e.g., the point of 90% amplitude) can be searched. Finally, the transient response parameters are calculated based on the coordinates of the feature points to achieve the calibration. Therefore, the way to calculate steady-state values directly affects the accuracy of the transient performance calibration.

The research on transient performance calibration is still at an early stage in China. The common scheme is to record

Manuscript received 5 April 2022; revised 21 May 2022; accepted 7 June 2022. Date of publication 20 June 2022; date of current version 1 July 2022. The Associate Editor coordinating the review process was Dr. He Wen. *(Corresponding author: Ruoyu Wu.)*

Dong Li, Ruoyu Wu, Han Liu, and Dezhi Chen are with the State Key Laboratory of Advanced Electromagnetic Engineering and Technology, School of Electrical and Electronic Engineering, Huazhong University of Science and Technology, Wuhan 430074, China (e-mail: lidonghust@hust.edu.cn; m202071706@hust.edu.cn; liuhan2772501364@163.com; dzhchen@hust.edu.cn).

Junchang Huang, Haoliang Hu, and Qi Nie are with the China Electric Power Research Institute, Wuhan 430074, China (e-mail: huang_jun_chang@qq.com; huhaoliang@epri.sgcc.com.cn; nieqi@epri.sgcc.com.cn).

Digital Object Identifier 10.1109/TIM.2022.3184350

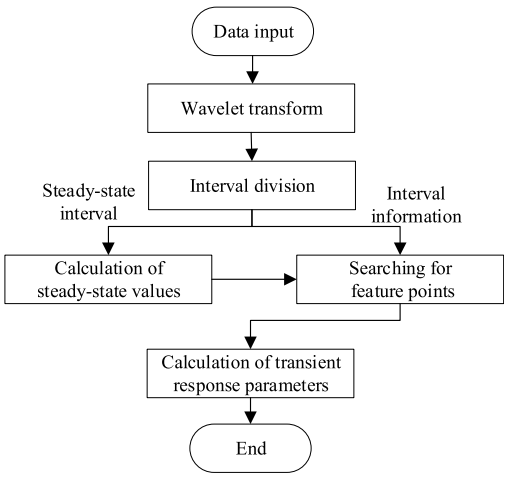

Fig. 2. Flowchart of the transient response performance analysis.

the waveform with a digital wave recorder at first in [10] and then find the step intervals, mark the amplitude and feature points of the waveform manually, and, finally, calculate the transient response parameters. The accuracy of the result is easily affected by human factors. A calibration platform based on the National Instrument (NI) sampling card is built in [11]–[13], in which the boundary window method is used to calculate steady-state values. First, it searches the midpoint of 50% amplitude roughly and then finds two boundary points on its left- and right-hand sides, respectively, whose distance to the midpoint depends on the period of square-wave response. Next, it sets two small windows from each boundary point toward the midpoint, respectively, and the data inside are used to calculate steady-state values. However, this method still needs to input some parameters manually, including the width of the boundary window and the period of the tested square-wave response. Moreover, it does not recognize the step and steady-state intervals automatically and search for suitable locations to set the boundary windows, which results in its inadequate applicability to different waveforms. Besides, this method does not evaluate the stability of the data within the window and adjust the window width adaptively, which may reduce the accuracy of calculated steady-state values.

A self-adaptive algorithm of the transient performance analysis for DCEIT calibration is proposed, which aims to recognize the characteristics of the square-wave response and distinguish the step and steady-state intervals automatically. By evaluating the stability of the data in steady-state intervals, it finds stable data segments to calculate the accurate steady-state values, which is beneficial for the subsequent data processing and analyses such as searching feature points, so as to achieve a comprehensive and accurate analysis of transient performance.

II. Design of the Self-Adaptive Algorithm

For different square-wave response waveforms, the characteristics are different, such as the length of the step or steady-state intervals, the step amplitude, and the oscillation characteristics. The flowchart of the proposed self-adaptive transient analysis algorithm is shown in Fig. 2. First, it uses the wavelet transform to recognize the characteristics of the square-wave response and distinguish the step and steady-state intervals automatically, which helps to position the data segments used to calculate the steady-state values. In addition, the widths of the data segments are adjusted adaptively by evaluating the data stability inside, so the accurate high and low steady-state values can be calculated. In the following chapters, the single-step response is taken as an example to illustrate the proposed algorithm clearly.

A. Method of Adaptive Interval Division

The step and steady-state intervals differ in both the time and frequency domains, which is the key to distinguish them. Wavelet transform has been widely used to detect the abrupt changes of transient signals in the electrical power system [14], [15]. Different from the Fourier transform, the wavelet transform provides a variable time–frequency window, which can focus on the local details of the signal in the time domain, so it is suitable for the recognition of step characteristics. Function $\varphi(t)$ with a mean of zero can be called a wavelet basis if its Fourier transform $\hat{\varphi}(t)$ satisfies the admissibility condition

$$C_\varphi = \int_R \frac{|\hat{\varphi}(\omega)|^2}{|\omega|} d\omega < \infty. \tag{1}$$

For a signal function $f(t)$ with limited energy, the wavelet coefficients WT_f can be calculated by wavelet transformation

$$\mathrm{WT}_f(s,\tau) = \frac{1}{\sqrt{|s|}} \int_{-\infty}^{+\infty} f(t) \cdot \varphi\left(\frac{t-\tau}{s}\right) dt \tag{2}$$

where τ and s are called the shift and scale of the wavelet basis, respectively, which reflects the time and frequency corresponding to the wavelet transformation. By changing the values of τ and s, the signal can be analyzed from both the time domain and the frequency domain at the same time to achieve the singularity detection of the step signal [16]. When the scale is s_0, if the following conditions are met in the neighborhood of point τ_0:

$$\left|\mathrm{WT}_f(s_0,\tau)\right| \le \left|\mathrm{WT}_f(s_0,\tau_0)\right| \tag{3}$$

then the modulus of WT_f (τ_0, s_0) is called the wavelet transform modulus maxima (WTMM). WTMM point can reflect the position of the abrupt change, and its polarity and amplitude reflect the direction and intensity of the change, respectively [17]. In the steady-state interval, the waveform changes smoothly, and the wavelet coefficient moduli are extremely small. In the step interval, the waveform changes rapidly and the modulus gradually increases, so that the WTMM point would appear at this interval. This principle can be used to recognize the step characteristics and then distinguish the step and steady-state intervals.

The selection of the wavelet basis directly affects the recognition ability, so it is necessary to select a suitable wavelet basis to acquire good results. When using the wavelet transform to achieve the interval division of the step waveform, the key is to find the position of the abrupt change. Therefore, the selected wavelet basis should be compactly supported,

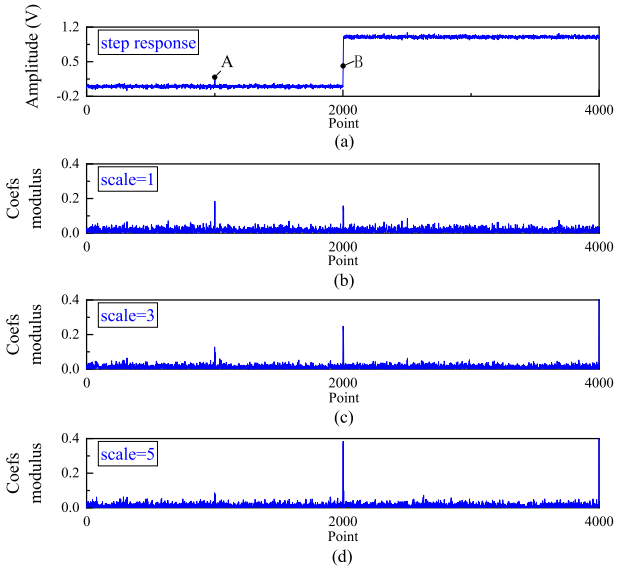

Fig. 3. Original signal and corresponding wavelet coefficient modulus. (a) The original step response waveform. (b) The wavelet coefficient modulus under the scale of 1. (c) The wavelet coefficient modulus under the scale of 3. (d) The wavelet coefficient modulus under the scale of 5.

so as to focus on the acquisition of information in the time domain [18]. The Haar wavelet with one support length is adopted, and its expression is given as follows:

$$\varphi_0(t) = \begin{cases} 1, & 0 \le t < \dfrac{1}{2} \\ -1, & -\dfrac{1}{2} \le t < 1 \\ 0, & \text{others.} \end{cases} \tag{4}$$

Most disturbances in the power system can be regarded as the disturbance model of the white noise [19], [20], which may also exist in the transient performance calibration site for the DCEIT. The randomness of noise can also cause the appearance of WTMM; therefore, it is necessary to distinguish between useful pulses and noise interferences. Lipschitz exponent is used to describe the local singularity of the function. For the signal function $f(t)$, if there is a positive integer A and nth degree polynomial $p_n(t)$, and the following conditions are satisfied in the neighborhood of t_0:

$$|f(t_0+h) - p_n(t_0+h)| \le A|h|^{\alpha}, \quad \alpha \in (n, n+1). \tag{5}$$

Then, α is called the Lipschitz exponent of $f(t)$ at t_0. Mallat and Hwang [21] and Yang [22] combined the Lipschitz exponent with the variation trend of the WTMM at different scales and obtained a theorem for distinguishing useful step signals from noise (especially white noise) interferences. The Lipschitz exponent of the useful step signal is greater than zero, and its WTMM is positively correlated with the scale of wavelet analysis. Conversely, the Lipschitz exponent of the white noise is less than zero, and its WTMM is negatively correlated with the scale. In a step response waveform with noise, the relationship between the wavelet coefficient modulus and scale is shown in Fig. 3. It can be seen that point A is the abrupt-change point of the white noise, and point B is the step point of the useful step signal.

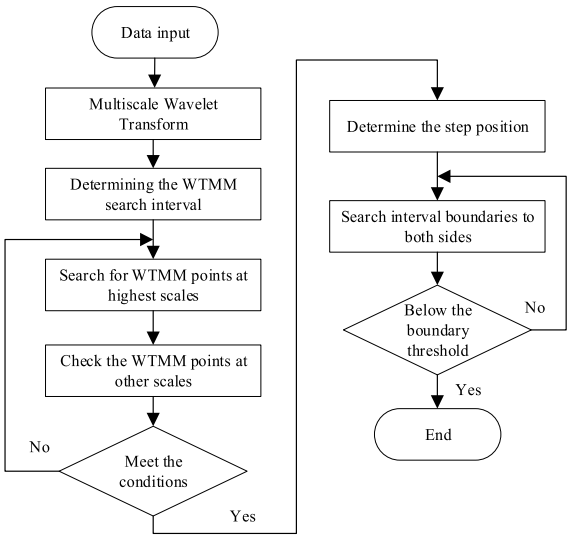

Fig. 4. Flowchart of the interval division.

Combining the theorem above with the distribution characteristics of the wavelet coefficients in the time domain, a flowchart of the adaptive interval division is proposed, as shown in Fig. 4. The detailed steps are given as follows.

1) Search the data segments that may contain the useful step points. Use the continuous wavelet transform to process the measured step response signal and obtain the wavelet coefficients at different scales. Then, search for the maximum and minimum modulus (i.e., $W_{s\max}$ and $W_{s\min}$) of wavelet coefficients at the highest scale $s_{\max}$

$$\begin{cases} W_{s\max} = \max\left|\mathrm{WT}_f(s_{\max}, \tau)\right| \\ W_{s\min} = \min\left|\mathrm{WT}_f(s_{\max}, \tau)\right|. \end{cases} \tag{6}$$

To avoid the interference of ringing on the recognition of the step feature, a scale factor β is set to define a threshold W_{flat} and intervals R_τ for searching for the WTMM point. In the subsequent test, β is set to 80%

$$W_{\text{flat}} = \beta |W_{s\max}| \tag{7}$$

$$R_\tau = \{\tau \,||\mathrm{WT}(s_{\max}, \tau)| \ge W_{\text{flat}}\}. \tag{8}$$

1) Screen out the moment when the useful step feature appears. Use (7) and (8) to find the WTMM point $A_{\max}$ $(\tau_a,\ WF_a)$ in R_τ at the highest scale. At other scales, the wavelet coefficients at τ_a are judged as follows. First, they should also be WTMM in their epsilon neighborhood. Second, their polarity is consistent with that of WF_a. Finally, the value of WTMM is positively related to the scale. If the conditions above are met, τ_a can be considered as the moment when the useful step appears.
2) Set a wavelet coefficient modulus threshold for interval division. At the highest scale, count the total number N_t of wavelet coefficients, divide the wavelet coefficients from $W_{s\min}$ to $W_{s\max}$ into small sections of n components with the equal magnitude, and then count the number N_i of wavelet coefficients contained in each component. The steady-state interval of the step response waveform is much longer than the step interval, so it contains most of the wavelet coefficients. Suppose the kth component has the

largest number N_k, and the proportion exceeds 90%

$$\frac{N_k}{N_t} \cdot 100\% > 90\%, \quad k = 1, 2, \quad \ldots, n. \tag{9}$$

Then, take the upper limit of this component as the steady-state judgment threshold W_{end}

$$W_{\text{end}} = W_{s\min} + k \cdot \frac{W_{s\max} - W_{s\min}}{n}. \tag{10}$$

1) Distinguish the steady-state and step intervals. Overshoot and ringing usually exist in the actual step response. Therefore, for the wavelet coefficient moduli at the highest scale, it is necessary to search from τ_a to both sides until the modulus is smaller than W_{end} continuously within a certain length. Then, the step interval $R_{\text{step}} = [\tau_1, \tau_2]$ can be determined

$$\begin{cases} \tau_1 = \max t_1, \\ t_1 \in \{t | \forall L \in (0, L_1], |WF(s_{\max}, t-L)| \le W_{\text{end}}, \ t < \tau_a\} \\ \tau_2 = \min t_2, \\ t_2 \in \{t | \ \forall L \in (0, L_2], |WF(s_{\max}, t+L)| \le W_{\text{end}} \ t > \tau_a\} \end{cases} \tag{11}$$

where L_1 and L_2 are the preset judgment lengths when searching forward and backward, respectively. According to the GB/T 26216.1-2019 standard, the setting time of the step response should not exceed 5 ms; therefore, it is appropriate to set L_2 to 8 ms and L_1 to 2 ms in the subsequent test. The interval before the step interval is regarded as the low steady-state interval, and the interval after is regarded as the high steady-state interval.

B. Method of Steady-State Values' Calculation

The high and low steady-state values of the step response waveform are very important because they directly affect the calculation of the amplitude and the search for feature points. On the basis of the interval division above, data segments of small fluctuation (i.e., reference interval) in each steady-state interval can be found, which are taken as the data source to calculate the steady-state values.

The first step is to determine the reference interval. Suppose that there are $2n + 1$ points in a steady-state interval (if the number is an even value, discard the first point), the corresponding amplitudes of the step waveforms are y_i ($i = 0$, 1, …, $2n$), and the midpoint is P_c (n, y_n). The length of the reference interval is set as $2m+1$ ($m \le n$), and the center is set at the point P_c. Trim both boundaries of the reference interval (i.e., reduce m from n to 1) until the following conditions are met at the first time:

$$\begin{cases} \bar{y}_m = \dfrac{\sum_{i=n-m}^{n+m} y_i}{2m+1}, \quad m = 1, \ldots, n \\ \max\left|\dfrac{y_i - \bar{y}_m}{\bar{y}_m}\right| \cdot 100\% \le \gamma\,\%, \quad i = n-m, \ldots, \quad n+m \end{cases} \tag{12}$$

where $\bar{y}_m$ is the average value of the reference interval, and γ is a threshold. In this way, the reference interval [n-m, $n + m$] is determined. According to the GB/T 26216.1-2019 standard, if the fluctuation range of the response amplitude is within ±1.5%, it is believed that the response enters the steady state. Thus, we can take the 1.5% as a threshold value for determining the reference interval.

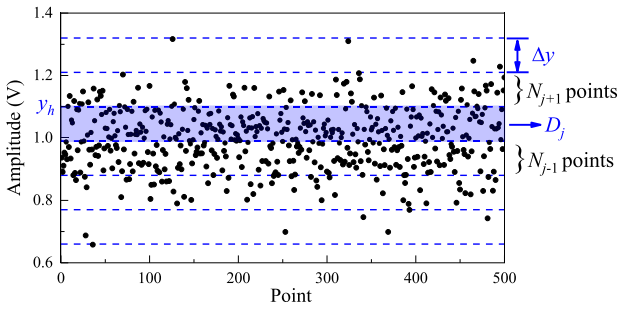

Fig. 5. Density distribution mode method for steady-state value calculation.

After that, the steady-state value is calculated based on the density distribution mode method. According to the amplitude variation range in the reference interval, all the data points are divided into several groups (D_0, D_1, …, D_k) of equal amplitude width Δy, as shown in Fig. 5. Count the number of points in each group, and the mode can be located in D_j; then, the steady-state value y_s is

$$y_s = y_h - \frac{N_{j-1}}{N_{j+1} + N_{j-1}} \cdot \Delta y \tag{13}$$

where y_h is the upper limit of the amplitude of D_j, and N_{j+1} and N_{j-1} are the numbers of points of the up and down adjacent groups, respectively. Calculate y_s in both high and low steady-state intervals, respectively, to obtain the high and low steady-state values y_∞ and y_0, and then, the accurate step amplitude can be obtained by subtracting y_∞ and y_0.

The feature points are of specific amplitude percentages, and transient response parameters, such as rise time and overshoot, can be calculated based on the coordinates of the feature points. For example, the rise time is the time difference between the feature points P_m (t_m, 90%) and P_n (t_n, 10%) in the step interval. However, the step response in the VSC-HVdc system lasts only tens to hundreds of microseconds usually, so the number of sampling points in the step interval is small, which means that the required feature points are usually not in the existing points. The cubic Hermite interpolation method is adopted to interpolate the step interval to improve the equivalent sampling rate at first. In this case, only a few feature points are contained in the interpolated data sequence. For the other feature points, linear interpolation is used further. Suppose that a feature point P (t_x, y_x) with an amplitude percentage of x% is between the equivalent sampling points P_1 (t_1, y_1) and P_2 (t_2, y_2); then, t_x and y_x can be calculated

$$y_x = (y_\infty - y_0) \cdot x\% + y_0 \tag{14}$$

$$t_x = t_1 + \frac{y_x - y_1}{y_2 - y_1} \cdot (t_2 - t_1). \tag{15}$$

III. Performance Evaluation

A. Simulation Test

According to the GB/T 26216.1-2019, for a qualified TUT, the rise time and overshoot of its step response should be less than 100 μs and 20%, respectively. Therefore, the self-adaptive

TABLE I

DETAILED PARAMETERS OF THE RESPONSE WAVEFORMS

Index	Amplitude /V	Overshoot /%	Rise time /μs	Setting time /μs
A	1	19.126	10	282.414
B	5	31.447	30	684.593
C	5	6.375	50	219.544
D	10	15.574	80	550.991
E	3	21.668	120	495.619
F	8	0	50	97.382

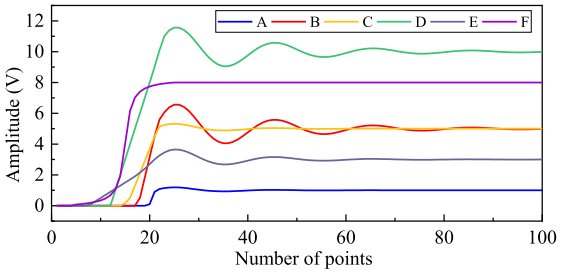

Fig. 6. Local details of the waveforms used for the test.

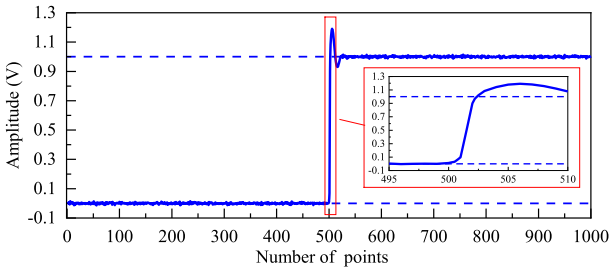

Fig. 7. One of the steps of the square-wave response A with noise.

algorithm of the transient performance analysis in the calibrator should be able to analyze the step response of a rise time ranges from 0 to 100 μs, and the overshoot ranges from 0% to 20% at least.

Six kinds of square-wave response waveforms are used to test the self-adaptive algorithm, whose local details within one period are shown in Fig. 6, and specific parameters are shown in Table I.

The white Gaussian noise with a signal-to-noise ratio (SNR) of 50 dB will be added to these responses, respectively, to simulate the noise interference that may exist in the actual test. The data of the tested waveforms are generated by MATLAB, and each waveform lasts for 1 s with ten rising edges, whose period is 0.1 s with a 50% duty cycle and the sampling rate is 100 kHz. The test data are imported into a LabVIEW software, in which the self-adaptive algorithm is embedded.

Take response A as an example. First, the original step waveform A without noise is put into the software, and the analysis results from the algorithm are shown in Table II. The relative errors of the parameters are extremely small, which proves the high accuracy of the algorithm in calculating transient response parameters. Second, its waveform with the white Gaussian noise shown in Fig. 7 is analyzed, and the results are shown in Table II and Fig. 8, in which the dotted lines are the real values of the parameters. The results show

TABLE II

TEST RESULTS OF THE WAVEFORM A WITH/WITHOUT NOISE

Parameters	Without noise		With 50dB gauss white noise	
	Value (μs)	Max relative error (%)	Average value (μs)	Max relative error (%)
Overshoot	19.151	0.131	19.175	0.810
Rise time	10.063	0.630	10.108	1.980
Setting time	282.452	0.014	282.682	1.123

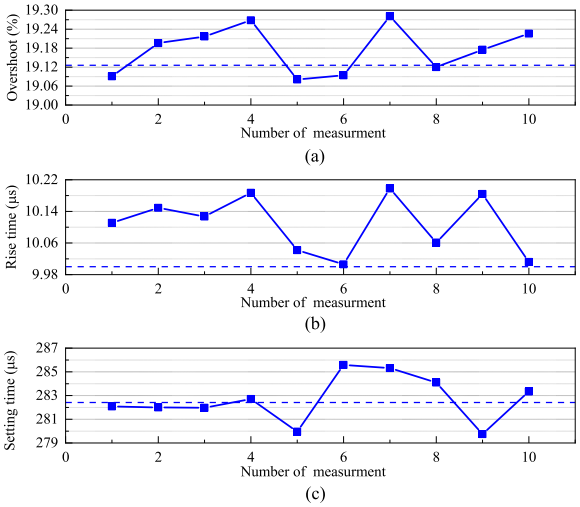

Fig. 8. Measured results of the waveform A. (a) Results of the overshoot. (b) Results of the rise time. (c) Results of the setting time.

TABLE III

ERROR OF THE TRANSIENT RESPONSE PARAMETERS

Index	Overshoot		Rise time		Setting time	
	Average (%)	Max relative error (%)	Average (μs)	Max relative error (%)	Average (μs)	Max relative error (%)
A	19.175	0.810	10.108	1.980	282.682	1.124
B	31.334	-0.795	30.032	-0.340	686.608	1.223
C	6.372	-2.203	50.107	0.894	218.871	-2.210
D	15.643	1.137	80.028	0.635	550.303	-0.808
E	21.698	-1.851	120.148	0.359	497.438	1.556
F	-0.015	/	49.987	-0.124	96.975	0.618
A'	18.961	-1.630	10.229	2.532	277.627	-2.173
B'	30.260	-5.728	29.945	1.466	676.105	-1.532
C'	6.235	-2.196	49.735	-1.125	215.688	-4.826
D'	15.033	-3.779	80.090	1.374	557.129	1.666
E'	21.149	-3.195	121.368	1.197	486.534	-2.398
F'	-0.017	/	49.886	-0.328	97.564	0.494

that the overshoot ranges from 19.081% to 19.281%, the rise time ranges from 10.006 to 10.198 μs, and the setting time ranges from 279.749 to 285.587 μs, but their relative errors are still at a low level. Thus, it proves that the algorithm has the ability of anti-interference to noise and can accurately calculate the parameters of the transient response.

In order to verify the self-adaptive ability of the algorithm, the other response waveforms in Table I with the white Gaussian noise are also tested. The results are shown in Table III, where indices A–F in the table represent the measurement results of the proposed algorithm. In addition, the above waveforms are also analyzed by the boundary window method for comparison, and indices A′–F′ in Table III are its results. Before the test, some parameters required by the

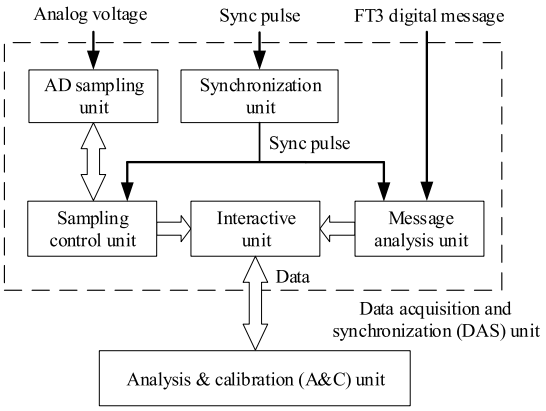

Fig. 9. Structure diagram of the calibrator prototype.

boundary window method should be preset. The waveform period is set to 0.1 s, and the window width is set to 0.04 s.

For the proposed algorithm, the relative errors of the overshoot, rise time, and setting time do not exceed 2.3%, 2.0%, and 2.3%, respectively. By contrast, for the boundary window method, the relative errors of these parameters are within 5.8%, 2.6%, and 4.9%, respectively, which are larger than that of the proposed algorithm. It is because the fixed width of the window may affect the calculation of the steady-state values. Thus, compared with the boundary window method, the proposed algorithm can calculate the transient response parameters automatically and is of higher accuracy in the cases above.

B. Calibrator Prototype Test

A calibrator prototype based on the proposed algorithm is developed, and its structure is shown in Fig. 9. The prototype is composed of a data acquisition and synchronization (DAS) unit and an A&C unit. ADS8881 is selected as the AD converter, which has 500 kSPS and 18-bit accuracy. The core controller of the DAS unit is an FPGA, whose function is to packet two-channel data and upload them to the A&C unit through the Ethernet. The A&C unit is developed based on LabVIEW, and the proposed algorithm is embedded for the transient performance analysis.

According to the transient performance calibration scheme in Fig. 1, a test platform for the calibrator prototype is built in the National Center for High Voltage Measurement (NCHVM), as shown in Fig. 10. A calibrator verification device is used to generate a known analog and corresponding FT3 digital signal, and the transient performance analysis results of the two signals are output by the prototype. The performance of the prototype is evaluated by comparing the analysis results with the waveform parameters provided by the verification device.

The verification device mainly consists of a signal generator AFG 3252C, a message sending device, and a control host. The rise time, overshoot, and setting time of the waveforms can be set by the control host. According to the inspection report from a third party, the amplitude error of the analog channel is less

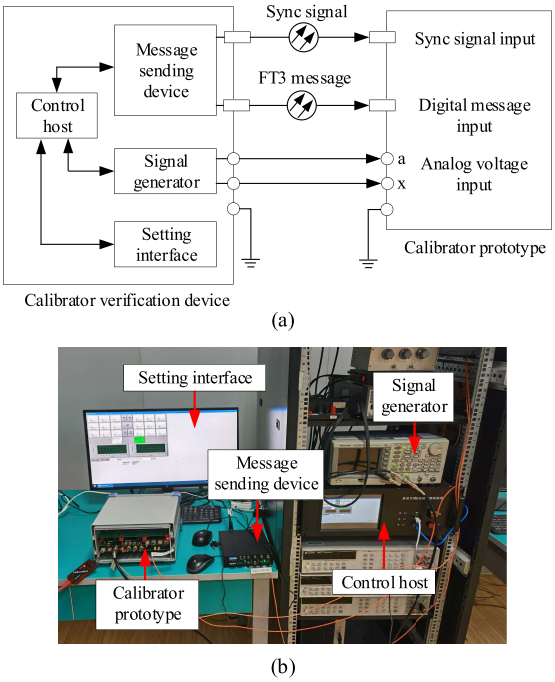

Fig. 10. Verification test of the calibrator prototype. (a) The verification test scheme diagram. (b) The verification test site.

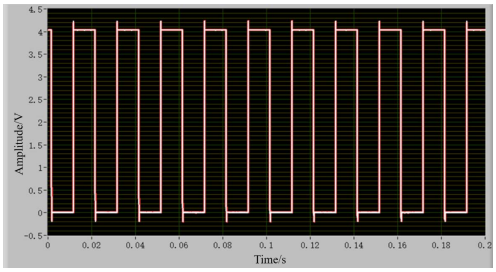

Fig. 11. Sampled data waveform of the square-wave signal H.

TABLE IV
DETAILED PARAMETERS OF THREE SQUARE-WAVE SIGNALS

Index	Overshoot /%	Rise time /μs	Setting time /μs
F	19.9	24.7	101.7
G	10.1	53.1	92.2
H	4.9	33.4	59.8

than 0.7%, and the time error is less than 1 μs. For the digital channel, the amplitude error is less than 1.5%, and the time error is less than 2.5 μs.

Three kinds of square-wave signals with different transient parameters are output by the verification device, as shown in Table IV, and each signal is measured at 25 rising edges at least. Fig. 11 shows the sampled data waveform of the signal H, and Table V shows the analysis results of the two channels. F1, G1, and H1 in the table represent the results of the analog channel; F2, G2, and H2 represent that of the digital channel.

For the analog channel, the relative errors of the overshoot, rise time, and setting time are about 1.6%, 0.8%, and 3.8%,

TABLE V
TEST ANALYSIS RESULT OF THE ANALOG/DIGITAL CHANNELS

Index	Overshoot		Rise time		Setting time	
	Average (%)	Relative error (%)	Average (μs)	Relative error (%)	Average (μs)	Relative error (%)
F1	19.591	-1.553	24.848	0.599	103.788	2.053
G1	10.074	-0.816	53.481	0.715	90.289	-2.073
H1	4.958	1.184	33.346	-0.180	57.586	-3.712
F2	18.524	-6.915	26.487	7.235	104.101	2.361
G2	9.551	-5.432	53.332	0.437	86.046	-6.674
H2	4.587	-6.531	34.073	2.006	57.745	-3.437

respectively. For the digital channel, the relative errors of these parameters are about 7.0%, 7.3%, and 6.7%, respectively. The analysis accuracy of the analog channel is higher than that of the digital channel. One of the reasons is that the sampling rate of the digital channel is 100 kHz and is lower than that of the analog channel, which limits the restoration effect on the original waveform.

IV. CONCLUSION

A self-adaptive algorithm of the transient response performance analysis is proposed, which is designed to analyze transient parameters of different step response waveforms without human intervention. Based on the wavelet analysis, the function of recognizing the steady-state and step intervals in the square-wave response automatically is achieved first. By evaluating the data stability in the steady-state interval and adaptively adjusting the reference interval, accurate steady-state values and step amplitude are obtained. Next, the data in the step interval are interpolated, and the feature points are searched accurately. Finally, accurate analysis of transient performance is completed.

The accuracy and self-adaptive ability of the algorithm are verified through a simulation test and a prototype test. In the simulation test, six square-wave response waveforms are used to validate the proposed algorithm, and the boundary window method is regarded as a comparison. For the proposed algorithm, the relative errors of the overshoot, the rise time, and the setting time do not exceed 2.3%, 2.0%, and 2.3%, respectively, which are more accurate than that of the boundary window method. In the NCHVM, a calibrator prototype based on the proposed algorithm is tested with a calibrator verification device. For the analog channel, the relative errors of the overshoot, the rise time, and the setting time are about 1.6%, 0.8%, and 3.8%, which are close to the results of the simulation test. The results show that the proposed algorithm can recognize the features of the square-wave response waveforms automatically without human intervention and achieve accurate analysis of transient performances. The research provides a self-adaptive algorithm of transient performance analysis for DCEIT calibration.

REFERENCES

[1] X. Y. Pei, G. Tang, and S. Zhang, "A novel pilot protection principle based on modulus traveling-wave currents for voltage-sourced converter based high voltage direct current (VSC-HVDC) transmission lines," *Energies*, vol. 11, no. 9, pp. 2315–2395, Sep. 2018, doi: 10.3390/en11092395.

[2] C. Hao *et al.*, "Discharge characteristics of DC system in Zhoushan multi-terminal VSC-HVDC transmission project," *High Voltage Eng.*, vol. 43, no. 1, pp. 9–15, Jan. 2017, doi: 10.13336/j.1003-6520.hve.201161227002.

[3] J. Zhang *et al.*, "Critical technology and equipment development of protection characteristics test of DC current transformer for VSC-HVDC transmission," *High Voltage Eng.*, vol. 44, no. 7, pp. 2159–2164, Jul. 2018, doi: 10.13336/j.1003-6520.hve.20180628007.

[4] H. Hu *et al.*, "Wide-range digital-analog mixed calibration technology of a DC instrument transformer test set," *IEEE Access*, vol. 9, pp. 75107–75116, 2021, doi: 10.1109/ACCESS.2021.3081144.

[5] *DC Current Measuring Device for HVDC Transmission System—Part 1: Electronic DC Current Measuring Device*, Chinese National Standard GB/T 26216.1-2019, 2019.

[6] F. Pang, Y. Liu, Q. Bu, and Q. Luo, "Research and application of transient step current source for DC current transformer on-site transient performance calibration," in *Proc. IEEE Int. Conf. Energy Internet (ICEI)*, Beijing, China, May 2018, pp. 269–274.

[7] L. Callegaro, C. Cassiago, and E. Gasparotto, "On the calibration of direct-current current transformers (DCCT)," *IEEE Trans. Instrum. Meas.*, vol. 64, no. 3, pp. 723–727, Mar. 2015, doi: 10.1109/TIM.2014.2359812.

[8] B. Djokic and E. So, "Calibration system for electronic instrument transformers with digital output," *IEEE Trans. Instrum. Meas.*, vol. 54, no. 2, pp. 479–482, Apr. 2005, doi: 10.1109/TIM.2004.843420.

[9] J. Zhang, G. Ye, and X. Liu, "Critical technology and equipment development of transient characteristics test on electronic current transformer for protection," *High Voltage Eng.*, vol. 43, no. 12, pp. 3884–3891, Dec. 2017, doi: 10.13336/j.1003-6520.hve.20171127009.

[10] J. Zhang *et al.*, "Critical technology of on-site calibration system for DC electronic instrument transformer," *High Voltage Eng.*, vol. 42, no. 9, pp. 3003–3010, Sep. 2016, doi: 10.13336/j.1003-6520.hve.20160907042.

[11] Q. Nie *et al.*, "Design of a transient calibration device and algorithm for DC transformer," *J. Shenyang Univ. Technol.*, vol. 42, no. 3, pp. 264–269, May 2020, doi: 10.7688/j.issn.1000-1646.2020.03.05.

[12] Q. Nie *et al.*, "A step response calibration system for DC current transformer," *Electr. Meas. Instrum.*, vol. 55, no. 19, pp. 112–118, Oct. 2018, doi: 10.3969/j.issn.1001-1390.2018.19.019.

[13] Q. Nie, H. Hu, D. Li, B. Liu, H. Li, and Q. Xiong, "Transient characteristics verification method for DC transformer used in flexible HVDC system," *Global Energy Interconnection*, vol. 2, no. 2, pp. 180–187, Apr. 2019, doi: 10.1016/j.gloei.2019.07.010.

[14] A. Glowacz, "DC motor fault analysis with the use of acoustic signals, coiflet wavelet transform, and K-nearest neighbor classifier," *Arch. Acoust.*, vol. 40, no. 3, pp. 321–327, Sep. 2015, doi: 10.1515/aoa-2015-0035.

[15] P. K. Murthy, J. Amarnath, S. Kamakshiah, and B. P. Singh, "Wavelet transform approach for detection and location of faults in HVDC system," in *Proc. IEEE Region 10 3rd Int. Conf. Ind. Inf. Syst.*, Dec. 2008, pp. 1–6, doi: 10.1109/ICIINFS.2008.4798483.

[16] B. Ai and Y. P. Lu, "Traveling wave signal identification based on wavelet polarity of modulus maxima," *Power Syst. Technol.*, vol. 27, no. 5, pp. 55–57 and 71, May 2003, doi: 10.3321/j.issn:1000-3673.2003.05.014.

[17] G. Sun *et al.*, "Research on an improved double-terminal traveling wave fault location method for UHVDC project," *Power Syst. Protection Control*, vol. 48, no. 14, pp. 113–120, Jul. 2020, doi: 10.19783/j.cnki.pspc.191050.

[18] Electrical Measurement & Instrumentation. (Jul. 28, 2020). *Research on the Characteristics of Wavelet Selection in Power Quality Signal De-Noising*. [Online]. Available: https://kns.cnki.net/kcms/detail/23.1202.TH.20200728.0838.002.html

[19] T. Huang, "Transient stability assessment of power system considering stochastic disturbances," M.S. thesis, Dept. Electron. Eng., Shanghai Jiao Tong Univ., Shanghai, China, 2019.

[20] X. Chen, "Research and application of harmonic detection in the power system," M.S. thesis, Dept. Electron. Eng., North China Electr. Power Univ., Beijing, China, 2019.

[21] S. Mallat and W. L. Hwang, "Singularity detection and processing with wavelets," *IEEE Trans. Inf. Theory*, vol. 38, no. 2, pp. 617–643, Mar. 1992, doi: 10.1109/18.119727.

[22] X. D. Yang, "Research on Extraction of ECG signal characteristic parameters based on wavelet transform," M.S. thesis, Dept. Electron. Eng., Univ. Electron. Sci. Technol. China, Chengdu, China, 2017.

Dong Li was born in Hubei, China, in 1982. He received the Ph.D. degree in electrical engineering from the Huazhong University of Science and Technology (HUST), Wuhan, China, in 2011.

He joined the School of Electrical and Electronic Engineering, HUST, in 2011, where he became an Associate Professor in 2017. His current research interests include digital metering and calibration.

Ruoyu Wu was born in Jiangxi, China, in 1997. He received the B.E. degree in electrical engineering from the East China University of Science and Technology, Shanghai, China, in 2019. He is currently pursuing the M.S. degree with the School of Electrical and Electronic Engineering, Huazhong University of Science and Technology, Wuhan, China.

His current research interests include digital metering and calibration.

Han Liu was born in Hubei, China, in 1997. He received the M.S. degree from the School of Electrical and Electronic Engineering, Huazhong University of Science and Technology, Wuhan, China, in 2021.

His research was on dc electronic instrument transformer calibration.

Junchang Huang was born in 1989. He received the M.S. degree in electrical engineering from the Huazhong University of Science and Technology (HUST), Wuhan, China, in 2014.

Since 2017, he has been a Research Engineer with the China Electric Power Research Institute, Wuhan. He is experienced in digital metering and calibration.

Haoliang Hu was born in Hubei, China, in 1984. He received the Ph.D. degree in electrical engineering from the Huazhong University of Science and Technology, Wuhan, China, in 2021.

He is currently a Senior Engineer with the China Electric Power Research Institute, Wuhan. His research interests include high-voltage and high-current metering, digital metering, calibration, and electronic instrument transformer applications.

Qi Nie was born in Jiangxi, China, in 1991. He received the B.S. and M.S. degrees in automation from the Wuhan University of Technology, Wuhan, China, in 2013 and 2015, respectively.

Since 2015, he has been a Research Engineer with the China Electric Power Research Institute, Wuhan. He is experienced in dc instrument transformer calibration technology and high-voltage measurement.

Dezhi Chen was born in 1969. He received the Ph.D. degree in electrical engineering from Xi'an Jiaotong University, Xi'an, China, in 1998.

He is currently a Professor with the School of Electrical and Electronic Engineering, Huazhong University of Science and Technology (HUST), Wuhan, China. His current research interests include electromagnetic field theory and numerical analysis.